Supporting Material for "Dynamics of forced nucleosome unraveling and role of nonuniform histone-DNA interactions"

Irina V. Dobrovolskaia and Gaurav Arya[1]

Department of NanoEngineering, University of California, San Diego, 9500 Gilman Drive, Mail Code 0448, La Jolla, CA 92093, U.S.A.

S1. Modeling of DNA

The DNA is treated using the discretized wormlike bead-chain model, where each "bead" represents a 3 nm segment of relaxed DNA (1, 2). Each bead is assigned a salt-dependent charge q_{dna} according to Stigter (3). The DNA bead-chain is also assigned an intramolecular force field comprising of stretching, bending, twisting terms that capture all aspects of DNA mechanics. The stretching energy U_{str} of the DNA is given by

$$U_{str} = \frac{h}{2} \sum_{i=1}^{N_{dna}-1} (l_i - l_0)^2 \tag{1}$$

where h is the stretching constant of DNA, N_{dna} is the total number of DNA beads, l_i is the length of the segment connecting beads i and $i+1$, and l_0 is the equilibrium segment length. The bending energy U_{ben} of DNA is given by

$$U_{ben} = \frac{g}{2} \sum_{i=1}^{N_{dna}-2} \beta_i^2 \tag{2}$$

where g is the bending constant of DNA derived from its persistence length and β_i is the Euler angle describing the angle between the neighboring segments connected by beads i and $i+1$ and by beads $i+1$ and $i+2$. The torsional energy U_{twi} of DNA is given by

$$U_{twi} = \frac{s}{2l_0} \sum_{i=1}^{N_{dna}-2} (\alpha_i + \gamma_i)^2 \tag{3}$$

where s is the torsional energy constant and α_i and γ_i are the Euler angles describing the twist between the local coordinate systems of adjacent DNA segments, respectively. The total electrostatic repulsion U_{rep} of the DNA is obtained as the sum of the Debye-Hückel potential between all interacting DNA beads, as given by

$$U_{rep} = \frac{q_{dna}^2}{4\pi\epsilon_0\epsilon} \sum_{i=1}^{N_{dna}-2} \sum_{j=i+2}^{N_{dna}} \frac{\exp(-\kappa r_{ij})}{r_{ij}} \tag{4}$$

where κ is the salt-dependent inverse Debye screening length, r_{ij} is the separation distance between beads i and j, and ϵ and ϵ_0 represent the dielectric constant of water and permitivity of vacuum. As the strong electrostatic repulsion prevents the DNA beads from overlapping with each other, no special excluded volume interactions are required. We use a monovalent salt concentration of 150 mM for parameterization and simulations.

[1]Correspondence: garya@ucsd.edu

The octamer is modeled as a rigid body composed of charged groove beads and neutral flanking and internal beads, as described in the main text. The charged groove beads interact with the DNA beads using the Debye-Hückel attractive potential:

$$U_{att} = \frac{q_{dna}}{4\pi\epsilon_0\epsilon} \sum_{i=1}^{N_{dna}} \sum_{j=1}^{N_{gr}} \frac{q_{oct,j} \exp(-\kappa r_{ij})}{r_{ij}} \tag{5}$$

where $q_{oct,j}$ denotes the charge on groove bead j and $N_{dna} = 39$ denotes the number of CG beads describing a 117 nm-long DNA used in our simulations. The groove, flanking, and interior beads interact with the DNA through an excluded volume potential treated using the Lennard-Jones (LJ) potential:

$$U_{ev} = 4\epsilon_{ev} \sum_{i=1}^{N_{dna}} \sum_{j=1}^{N_{oct}} \left[\left(\frac{\sigma_{ev}}{r_{ij}} \right)^{12} - \left(\frac{\sigma_{ev}}{r_{ij}} \right)^{6} \right] \tag{6}$$

where σ_{ev} and ϵ_{ev} are the LJ energy and size parameters, which are chosen to ensure that the DNA beads do not enter the interior of the histone octamer and that they do not overlap extensively with the oppositely charged groove beads. The total potential energy of the nucleosome is then given by the sum of the intramolecular DNA stretching, bending, torsion, and electrostatics terms and the intermolecular electrostatic and excluded volume interaction terms between the DNA and the octamer. The parameters for the above energy terms are provided in Table S1.

S2. Brownian dynamics simulations

We employ a Brownian dynamics approach to simulate the dynamics of the octamer and the DNA subjected to extensional forces. We account for friction but not explicit hydrodynamic interactions, whose effects are secondary to the primary phenomenon being investigated here. The second-order Runge-Kutta algorithm of Iniesta and de la Torre (2, 4) is employed for updating the translation $\mathbf{r}_i(t)$ and rotation vectors $\mathbf{\Omega}_i(t)$ of each component i of the system (i = DNA beads or rigid octamer):

$$\begin{aligned} \mathbf{r}_i(t+\Delta t) &= \mathbf{r}_i(t) + \frac{D_i^T(\mathbf{F}_i(t) + \mathbf{F}_i^*)}{2k_BT}\Delta t + \mathbf{R}_i \\ \mathbf{\Omega}_i(t+\Delta t) &= \mathbf{\Omega}_i(t) + \frac{D_i^R(\mathbf{T}_i(t) + \mathbf{T}_i^*)}{2k_BT}\Delta t + \mathbf{W}_i \end{aligned} \tag{7}$$

where D_i^T and D_i^R are the translation and rotational diffusion coefficient, respectively; $\mathbf{F}_i(t)$ and $\mathbf{T}_i(t)$ are the forces and torques experienced by component i at time t; $\mathbf{F}_i^*$ and $\mathbf{T}_i^*$ are the predicted force and torque at time $t + \Delta t$; and $\mathbf{R}_i$ and $\mathbf{W}_i$ are Gaussian-distributed random vectors satisfying the fluctuation-dissipation theorem:

$$\begin{aligned} \langle \mathbf{R}_i \rangle = 0, \qquad & \langle \mathbf{R}_i \mathbf{R}_j \rangle = 2D_i^T \Delta t \delta_{ij} \mathbf{I} \\ \langle \mathbf{W}_i \rangle = 0, \qquad & \langle \mathbf{W}_i \mathbf{W}_j \rangle = 2D_i^R \Delta t \delta_{ij} \mathbf{I} \end{aligned} \tag{8}$$

The above equations of motions apply for all components except the two terminal linker DNA beads, which are pulled at constant speeds $V_{pull}/2$ in opposite directions along the y-direction, as depicted in Fig. 1 A.

While the octamer exhibits rotation and torque along its three axes, the DNA beads only exhibit rotation and torque along their axis, defined by a vector pointing towards the next bead along the DNA bead-chain. The reader is referred to Ref. (2, 5) for a detailed description of the DNA model. The translational and rotational diffusion coefficient of the octamer is given by $D^T_{oct} = k_BT/6\pi\eta R_{oct}$ and $D^R_{oct} = k_BT/8\pi\eta R^3_{oct}$, where R_{oct} is the hydrodynamic radius of octamer and η is the solvent viscosity. Similarly, the translational and rotational diffusion coefficient of the DNA beads along the DNA axis $D^R_{dna} = k_BT/4\pi\eta R^2_{dna} l_0$, where R_{dna} is the hydrodynamic radius of each DNA bead and $l_0 \equiv 3$ nm is the segment length associated with each DNA bead. The force on each DNA and octamer bead is computed from the gradient of the total potential energy

$$\mathbf{F}_i = -\nabla_{\mathbf{r}_i} U_{tot} \tag{9}$$

where $\mathbf{r}_i$ and $\mathbf{F}_i$ are the position vector and force acting on component i, respectively. The torque on the ith DNA bead acting along its axis vector $\hat{\mathbf{a}}_i$, arising from the twisting potential, is given by

$$\mathbf{T}_{dna,i} = -\frac{s}{l_0}(\alpha_i + \gamma_i - \alpha_{i-1} - \gamma_{i-1})\hat{\mathbf{a}}_i \tag{10}$$

while the torque on the histone octamer is given by

$$\mathbf{T}_{oct} = \sum_{i=1}^{N_{oct}} (\mathbf{r}_i - \mathbf{r}_{cm}) \times \mathbf{F}_i \tag{11}$$

where $\mathbf{r}_i - \mathbf{r}_{cm}$ denotes the position vector of octamer bead i relative to the octamer center of mass. All parameters associated with the BD algorithm are provide in Table S1.

S3. Obtaining free energy contribution of each groove bead

The binding free energy contribution $\Delta G_{exp}(i)$ from each octamer groove bead i is derived from the DNA position-dependent cumulative free energy profile $G_{exp}(x)$ obtained by Forties et al. (6) (Fig. S1A). The DNA position x is defined relative to its nucleosomal entry site. Thus, the dyad and the nucleosome exit sites are located at $x = 73$ bp and $x = 146$ bp, respectively. Our procedure for obtaining $\Delta G_{exp}(i)$ consists of *four* steps. First, we shift the given profile by 73 bp such that the DNA position is now relative to the dyad axis; the shifted profile is denoted by $G_{sh}(x)$. Second, the provided profile is not symmetric about the dyad and is also incomplete on the right hand side of the dyad. To this end, we "symmetrize" the profile ± 10 bp about the dyad axis. Specifically, we replace the deviation in the free energy from its dyad value, i.e., $(G_{sh}(x) - G_{sh}(0))$, by the average value of the deviation in the left and right hand sides portions, i.e., $[(G_{sh}(x) - G_{sh}(0)) + (G_{sh}(0) - G_{sh}(-x))]/2$. The symmetrized profile, denoted by $G_{sym}(x)$, is then formally described by the following expression:

$$G_{sym}(x) = \begin{cases} G_{sh}(x) & \text{if } x < -10 \text{ bp} \\ \frac{1}{2}[G_{sh}(-10) + G_{sh}(10)] + \frac{1}{2}[G_{sh}(-x) - G_{sh}(x)] & \text{if } -10 \le x < 0 \text{ bp} \end{cases} \tag{12}$$

This symmetrized profile is shown in Fig. S1B. Third, we obtain a continuous free energy profile G_{fit} from G_{sym} through spline fitting via MATLAB (Fig. S1B). Fourth, we determine the free energies contributed by each octamer groove bead from the free energy difference along the span of the DNA length associated with each bead, which is equal to 8.59 bp (Fig. S1C). The derived free energy contribution ΔG_{exp} for each groove bead on the left hand side of the dyad is plotted as a function of bead location in Fig. S1D. The groove beads on the right

hand side can be obtained by symmetry: $\Delta G_{exp}(18-i) = \Delta G_{exp}(i)$, recalling that there are 17 groove beads in total.

S4. Derivation of groove charge magnitudes

The charge parameterization procedure outlined in the main text yielded Eqs. (2-5), which are rewritten below for convenience:

$$\Delta G_{exp} = \sum_{i=1}^{N_{gr}} \Delta U_{do}(i) + \Delta G_{rem} \quad (13)$$

$$\Delta G_{exp}(i) = \Delta U_{do}(i) + \Delta G_{rem}/N_{gr} \quad (14)$$

$$\Delta U_{do}(i) = -K q_{oct,i} \quad (15)$$

$$\Delta G_{exp} = \alpha \sum_{i=1}^{N_{gr}} \Delta U_{do}(i) \quad (16)$$

where $\Delta G_{exp} \equiv \sum_{i=1}^{N_{gr}} \Delta G_{exp}(i)$. Substitution of Eq. (14) into Eqs. (12) and (15) yields the following two equations:

$$\Delta G_{exp} = -K \sum_{i=1}^{N_{gr}} q_{oct,i} + \Delta G_{rem} \quad (17)$$

$$\Delta G_{exp} = -K\alpha \sum_{i=1}^{N_{gr}} q_{oct,i} \quad (18)$$

Substitution of Eq. (17) into Eq. (15) followed by simplification yields:

$$\Delta G_{rem} = K(1-\alpha) \sum_{i=1}^{N_{gr}} q_{oct,i} \quad (19)$$

Substitution of Eq. (17) into Eq. (18) yields:

$$\Delta G_{rem} = -\frac{1-\alpha}{\alpha} \Delta G_{exp} \quad (20)$$

Finally, substitution of Eqs. (14) and (19) into Eq. (13) yields:

$$\Delta G_{exp}(i) = -K q_{oct,i} - \frac{1-\alpha}{\alpha N_{gr}} \sum_{i}^{N_{gr}} \Delta G_{exp}(i) \quad (21)$$

Upon rearrangement, Eq. (20) yields the final expression we seek for parameterizing the octamer groove bead charges:

$$K q_{oct,i} = -\Delta G_{exp}(i) - \frac{1-\alpha}{\alpha N_{gr}} \sum_{i=1}^{N_{gr}} \Delta G_{exp}(i) \quad (22)$$

S5. Model for extrapolating unraveling forces

The theoretical model used in this study for extrapolating the computed unraveling forces to small pulling speeds was developed (7–9) to quantify the rates of transitions in molecules subjected to a linearly increasing force in time, as implemented in dynamic force spectroscopy. The molecular transitions could involve dissociation of molecular complexes held by intermolecular interactions—such as drug-receptor systems, double-stranded DNA, and DNA/protein complexes—to the unfolding of single molecules held together by secondary interactions—such as folded RNAs and proteins.

The model assumes that the molecular transition occurs in the high-friction limit, where the timescale of the transition is significantly longer than that associated with the thermalization of the molecule. Furthermore, the transition is assumed to occur along a single, dominant reaction coordinate, the pulling direction. Both assumptions are in fact applicable to the nucleosome unraveling transition. Under such circumstances, one can describe the molecular transition in terms of a potential of mean force (PMF) or the effective free energy along the reaction coordinate. The PMF of the unperturbed system along the coordinate x containing the stable bound state, the metastable dissociated state, and an energy barrier separating the two states was modeled using a linear-cubic polynomial $G_0(x)$ (Fig. S4). The effect of the force was modeled as a tilting of the energy landscape, yielding a new perturbed PMF: $G(x;F(t)) = G_0(x) - F(t)x$. This tilting results in a lowering of the barrier height and a reduction in the distance to the barrier (Fig. S4). The model then invoked Kramers theory, valid under the high-friction limit and large barrier heights, to determine the average transition rate $k(F)$ over the barrier as a function of the instantaneous force $F(t)$. Formulating the net rate of transitions across the barrier $dS(t)/dt$ as being equal to the transition rate $k(F)$ multiplied by the remaining fraction of bound states $S(t)$ then allows one to determine the distribution of times $p(\tau_{tr})$, and the distribution of forces $p(F_{tr})$, at which the transitions occur. The distribution $p(F_{tr})$ can also be averaged to provide the mean force $\langle F_{tr} \rangle$:

$$\langle F_{tr} \rangle = \frac{\Delta G^*}{\nu x^*} \left[1 - \left\{ \frac{1}{\beta \Delta G^*} \ln \frac{k_0 e^{\beta \Delta G^* + \gamma}}{\beta x^* \dot{F}} \right\}^{\nu} \right] \tag{23}$$

where ΔG^* is the height of the activation energy barrier associated with the transition, x^* is the distance between the barrier and bound state, k_0 is the intrinsic transition rate at zero force, $\dot{F}$ is the rate at which the imposed force is increasing (loading rate), and $\gamma = 0.578$, $\nu = 2/3$, and $\beta = 1/k_B T$.

Equation 20 can be directly applied to extrapolate the rupture forces F_{unr} computed at large pulling speeds to the small pulling speeds v_{pull} typically employed in single molecule pulling experiments. In our case, the molecular transition being examined is the abrupt unraveling of the nucleosome. Therefore, the fully wrapped nucleosome represents the bound state and the fully unwrapped nucleosome the dissociated state. The unraveling force F_{unr} takes the place of $\langle F_{tr} \rangle$. The pulling speed-dependent $\dot{F}$ is determined from the slope of the F-t curve before the abrupt unraveling transition. The remaining parameters such as the energy barrier, barrier location, and transition rate are the unknowns of the system that are adjusted within known bounds until the F_{unr}-$\dot{F}$ fit yields the least deviation between the computed and experimentally measured F_{unr}.

S6. Energetics of nucleosome unraveling

We have plotted in Fig. S2 the time evolution of the total energy U_{tot} of the nucleosome during unraveling along with that of its *five* components arising from DNA stretching (U_{str}), DNA bending (U_{ben}), DNA twisting (U_{twi}), electrostatic repulsion between DNA (U_{rep}), and DNA/octamer interactions ($U_{oct/dna}$), the last of which includes both electrostatic attraction and excluded volume interactions.

In regime $\mathcal{R}_1$, where the linkers are relaxed, U_{tot} exhibits minimal changes. The only changes that occur within this regime are a gradual decrease in U_{ben} due to straightening of the linkers and a small increase in $U_{oct/dna}$ within the early stages of the regime due to the unwrapping/rewrapping of the flanking portions of wound DNA. Note that the two energy changes do not include the loss in entropy incurred with linker straightening and the gain in entropy associated with DNA release.

In regime $\mathcal{R}_2$, where the linkers become taut, we note a sharp rise in U_{tot} until the unraveling of the inner turn (force rip). The main contributors to this rise are increases in $U_{oct/dna}$, U_{ben}, and U_{str} even though U_{rep} decreases. The increase in $U_{oct/DNA}$ and decrease in U_{rep} both arise from the unwrapping of the "outer" turn of DNA from the octamer. The increase in U_{str} arises from the DNA becoming taut while the increase in U_{ben} arises from the bending of DNA at the entry/exit point in order to align with the linkers, which are oriented along the pulling direction.

Upon the unwrapping of the "inner" turn, at the beginning of regime $\mathcal{R}_3$, the DNA becomes relaxed again and the DNA bending and stretching energies drop. Continued pulling of the linkers results in the DNA becoming taut, leading to an increase in the DNA stretching energy. However, the bending energy term remains constant, as the small amount of DNA still attached to the octamer is already aligned along the pulling direction and does not need to bend, as in regime $\mathcal{R}_2$. It is noted that the DNA twisting energy understandibly remains nearly constant throughout the pulling, as the DNA ends are free to rotate during pulling.

Supporting References

1. Dobrovolskaia, I. V., M. Kenward, and G. Arya. 2010. Twist propagation in dinucleosome arrays. *Biophys. J.* 99:3355–3364.

2. Arya, G., Q. Zhang, and T. Schlick. 2006. Flexible histone tails in a new mesoscopic oligonucleosome model. *Biophys. J.* 91:133–150.

3. Stigter, D. 1977. Interactions of highly charged colloidal cylinders with applications to double-stranded DNA. *Biopolymers.* 16:1435–1448.

4. Iniesta, A., and J. G. de la Torre. 1990. A 2nd-order algorithm for the simulation of the Brownian dynamics of macromolecular models. *J. Chem. Phys.* 92:2015–2018.

5. Arya, G., and T. Schlick. 2009. A tale of tails: How histone tails mediate chromatin compaction in different salt and linker histone environments. *J. Phys. Chem. A.* 113:4045–4059.

6. Forties, R. A., J. A. North, S. Javaid, O. P. Tabbaa, R. Fishel, M. G. Poirier, and R. Bundschuh. 2011. A quantitative model of nucleosome dynamics. *Nucleic Acids Res.* 39:8306–8313.

7. Dudko, O. K., G. Hummer, and A. Szabo. 2006. Intrinsic rates and activation free energies from single-molecule pulling experiments. *Phys. Rev. Lett.* 96:108101.

8. Maitra, A., and G. Arya. 2010. Model accounting for the effects of pulling-device stiffness in the analyses of single-molecule force measurements. *Phys. Rev. Lett.* 104:108301.

9. Maitra, A., and G. Arya. 2011. Influence of pulling handles and device stiffness in single-molecule force spectroscopy. *Phys. Chem. Chem. Phys.* 13:1836–1842.

10. Davey, C. A., D. F. Sargent, K. Luger, A. W. Maeder, and T. J. Richmond. 2002. Solvent mediated interactions in the structure of the nucleosome core particle at 1.9 Å resolution. *J. Mol. Biol.* 319:1097–1113.

Table S1: Physical parameters associated with the coarse-grained nucleosome and Brownian dynamics simulations.

Parameter	Description	Value
l_0	Equilibrium DNA segment length	3.0 nm
h	DNA stretching constant	$300 k_B T / l_0^2$
g	DNA bending constant	$L_p k_B T / l_0^2$
s	DNA torsional rigidity	300 pN nm^2
L_p	DNA persistence length	50 nm
σ_{ev}	Excluded volume size parameter	2.4 nm
ϵ_{ev}	Excluded volume energy parameter	0.025 $k_B T$
ϵ	Dielectric constant of solvent	80
q_{dna}	Charge on DNA beads	$-24.1e$
c_s	Salt concentration	150 mM
κ	Inverse Debye screening length	1.275 nm^{-1}
T	Temperature	300 K
R_{oct}	Hydrodynamic radius of octamer	4.0 nm
R_{dna}	Hydrodynamic radius of linker bead	1.5 nm
Δt	BD simulation timestep	2 ps
N_{gr}	Number of charged, groove beads	17
N_{flk}	Number of flanking beads	34
N_{cen}	Number of inner core beads	14
N_{oct}	Total number of octamer beads	65
N_{dna}	Total number of DNA beads	39
λ	Groove bead charge scaling factor	$7.1e$
w_{dna}	Width of wound DNA supercoil	4.5 nm
r_{dna}	Radius of wound DNA supercoil	4.18 nm

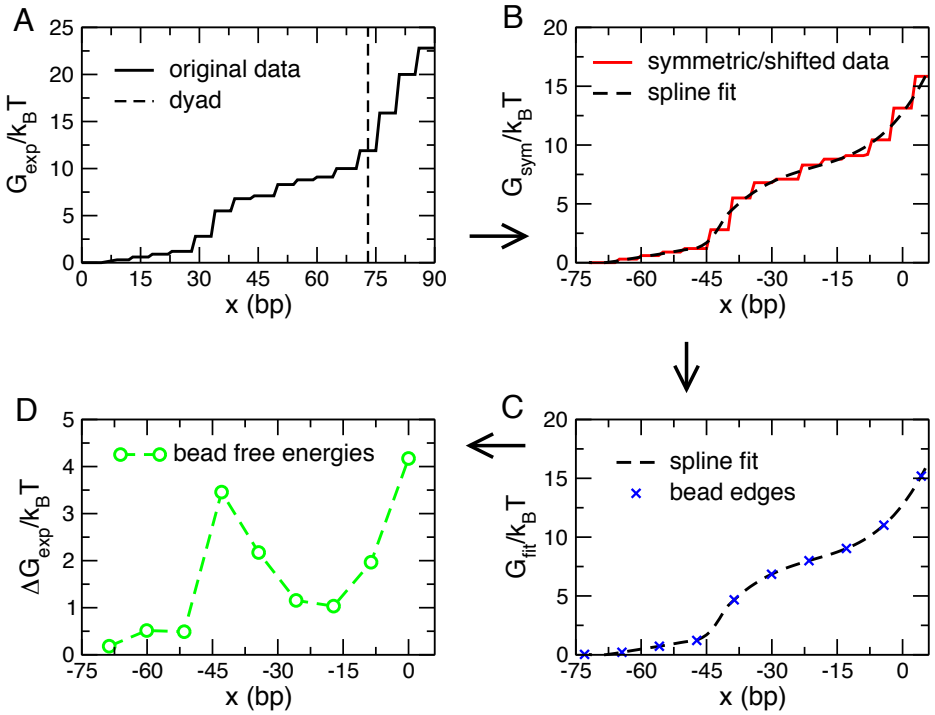

Figure S1: Procedure for deriving binding free energy contribution ΔG from each octamer groove bead. (A) Original cumulative free energy profile $G_{exp}(x)$ of Forties et al. (6) (black line). The dotted line represents the dyad location. (B) Shifted and symmetrized free energy profile $G_{sym}(x)$ (red line) and its spline fit $G_{fit}(x)$ (dashed black line). (C) Free energy profile indicating the span of the DNA segments associated with each groove bead, which are all equal to 8.59 bp (blue crosses). (D) Free energy contribution for each groove bead determined from the free energy difference across the DNA length associated with each bead (green circles).

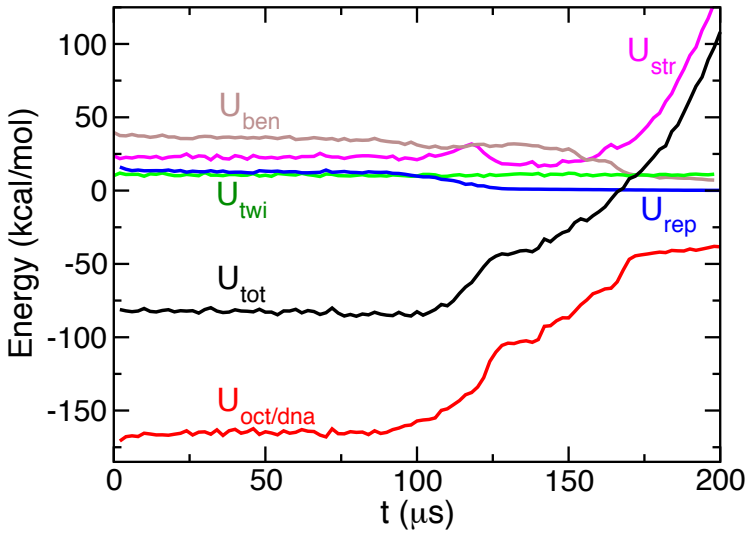

Figure S2: Time evolution of the total energy U_{tot} (black) of the nucleosome system (black line) and its four components from DNA stretching U_{str} (magenta line), DNA bending U_{ben} (brown line), DNA twisting U_{twi} (green line), and DNA/DNA repulsion U_{rep} (blue line), and DNA/octamer attraction $U_{oct/dna}$ (red line). For intact nucleosomes, at small times, DNA/octamer attraction $U_{oct/dna} \approx -168$ kcal/mol and the effective attraction $U_{tot} \approx -80$ kcal/mol. Thus, unfavorable contributions to DNA/histone binding from DNA stiffness and DNA/DNA repulsion, reduce the overall affinity of DNA for the octamer by a factor $\alpha = 1/2$.

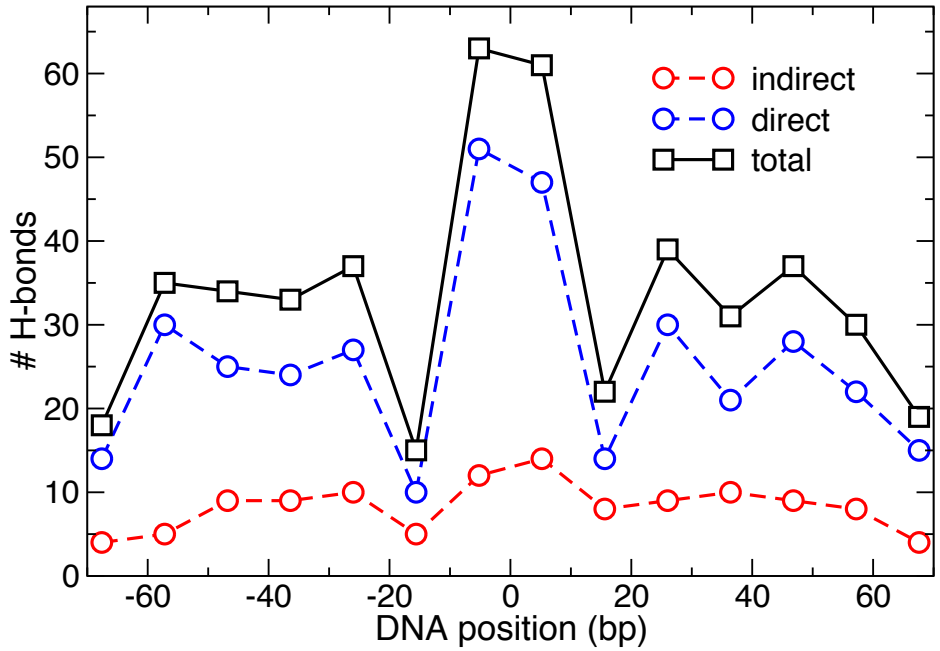

Figure S3: Number of direct and indirect hydrogen bonds between DNA and the histone octamer at different locations along the wound DNA, as obtained by Davey et al. (10).

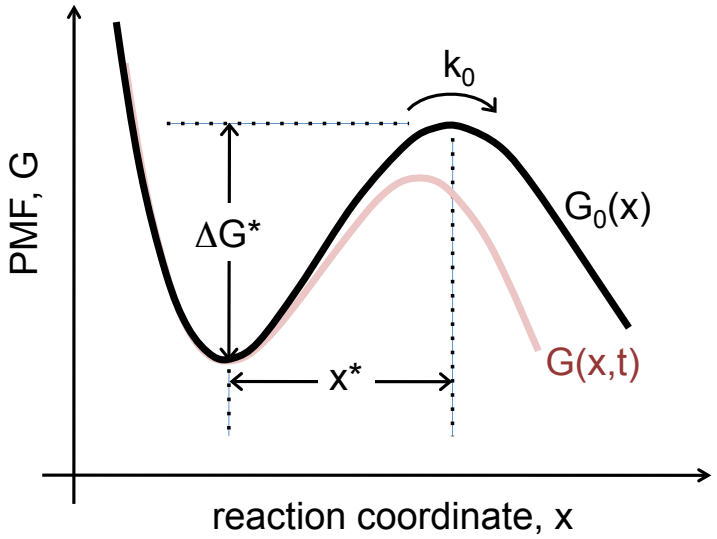

Figure S4: Force-induced tilting of the energy landscape. The intrinsic PMF $G_0(x)$ (black curve) with energy barrier ΔG^*, distance to barrier x^*, and transition rate k_0 tilts with imposed force F to a modified PMF $G(x, F)$ (brown curve) with a smaller energy barrier and smaller distance to barrier.

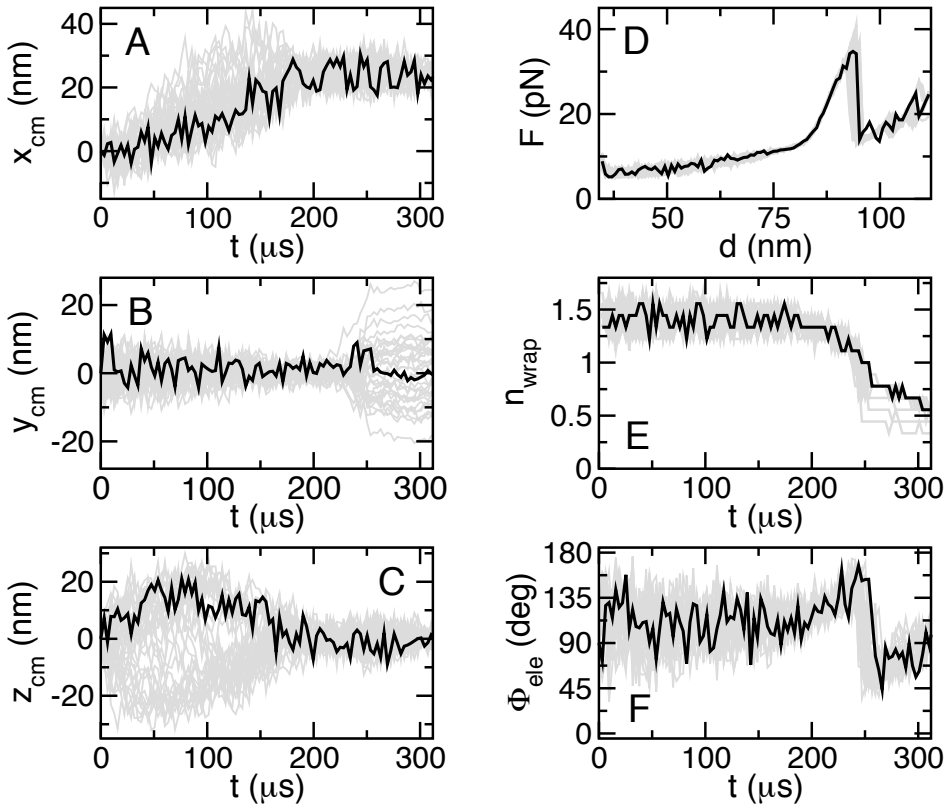

Figure S5: Results from unraveling simulations performed at $v_{pull} = 0.025$ cm/s. (A-C) Cartesian coordinates of the octamer center of mass as a function of time. (D) Force-extension curves. (E) Extent of nucleosome wrapping as a function of time. (F) Octamer elevation angle as a function of time. In each case, one representative trajectory is shown in black while the remaining 35 trajectories are shown in grey.

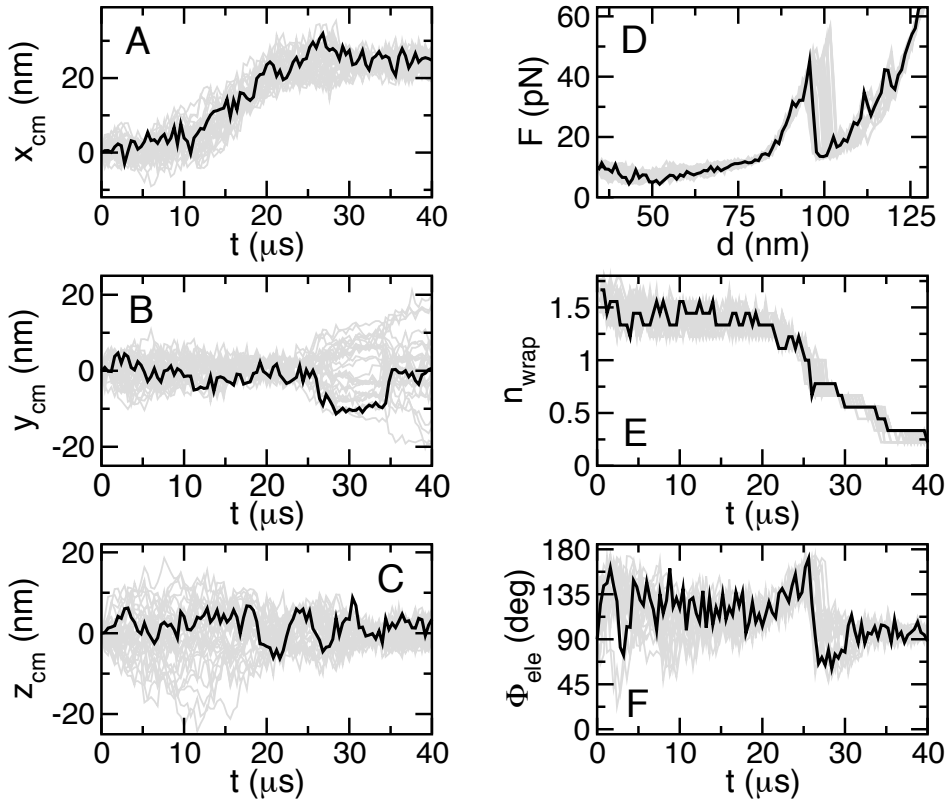

Figure S6: Results from unraveling simulations performed at $v_{pull} = 0.25$ cm/s. (A-C) Cartesian coordinates of the octamer center of mass as a function of time. (D) Force-extension curves. (E) Extent of nucleosome wrapping as a function of time. (F) Octamer elevation angle as a function of time. In each case, one representative trajectory is shown in black while the remaining 35 trajectories are shown in grey.